nature biomedical engineering

ARTICLES

PUBLISHED: 23 JANUARY 2017 | VOLUME: 1 | ARTICLE NUMBER: 0011

In situ activation of platelets with checkpoint inhibitors for post-surgical cancer immunotherapy

Chao Wang[1,2], Wujin Sun[1,2], Yanqi Ye[1,2], Quanyin Hu[1,2], Hunter N. Bomba[1] and Zhen Gu[1,2,3]*

Cancer recurrence after surgical resection remains a significant challenge in cancer therapy. Platelets, which accumulate in wound sites and interact with circulating tumour cells (CTCs), can however trigger inflammation and repair processes in the remaining tumour microenvironment. Inspired by this intrinsic ability of platelets and the clinical success of immune checkpoint inhibitors, here we show that conjugating anti-PDL1 (engineered monoclonal antibodies against programmed-death ligand 1) to the surface of platelets can reduce post-surgical tumour recurrence and metastasis. Using mice bearing partially removed primary melanomas (B16-F10) or triple-negative breast carcinomas (4T1), we found that anti-PDL1 was effectively released on platelet activation by platelet-derived microparticles, and that the administration of platelet-bound anti-PDL1 significantly prolonged overall mouse survival after surgery by reducing the risk of cancer regrowth and metastatic spread. Our findings suggest that engineered platelets can facilitate the delivery of the immunotherapeutic anti-PDL1 to the surgical bed and target CTCs in the bloodstream, thereby potentially improving the objective response rate.

Surgery is the main treatment option for most solid tumours. Despite continual improvements in surgical techniques, residual microtumours and/or circulating tumour cells (CTCs) after tumour resection remain a challenge[1–3]. In addition, it has also been suggested that surgery can induce the promotion of cancer metastasis[4,5]. Many patients develop recurrent disease post-surgery, which can lead to significant morbidity as well as mortality. Hence, there has been tremendous interest in developing effective strategies to prevent cancer recurrence after surgery. Among them, cancer immunotherapy has received considerable attention recently[6]. Immunotherapeutic agents boost the body's immune system to attack cancer cells, rather than destroy them directly[7]. Durable clinical response and long-term remissions have been elicited in a fraction of cancer patients treated with the immune checkpoint blockade (ICB)[8–10], working by preventing programmed-cell-death protein 1 (PD1) on T lymphocytes (T cells) from binding programmed-death ligand 1 (PDL1) on cancer cells and antigen-presenting cells (APCs), which would otherwise inactivate the lymphocytes and allow the cancer cells to evade attack. Use of such inhibitors has achieved exciting results in treating various types of cancer[11–14]. Moreover, the first PDL1 inhibitor, atezolizumab, has recently been granted accelerated approval by the US Food and Drug Administration (FDA)[15]. Despite remarkable progress, the current ICB-based treatments still have many limitations[16–18]. Side effects, such as autoimmune disorders, have often occurred in those undergoing ICB therapy[15,19]. Furthermore, the objective response rate of anti-programmed-death (anti-PD) therapy also needs improvement, with a large fraction of patients failing to respond to these agents[8,10,15]. Efforts to address these problems of anti-PD therapy have become one of the major themes in the field of cancer immunotherapy[6,11].

One mechanism that may account for the compromised efficacy of anti-PD therapy is off-target binding of antibodies to normal tissues when intravenously infused[16,18,20,21]. In this context, it is ideal for cancer immunotherapy to focus on the diseased site whilst preventing the systemic nonspecific over-activation of the immune system[20]. The limited efficacy may also be due to insufficient lymphocytic infiltration of the tumour and insufficient T-cell-induced inflammation in the tumour microenvironment[22–25]. Lymphocytic infiltration and the associated inflammation leads to increased expression of PDL1, which is positively associated with the clinical benefits of anti-PD therapy.

Cell-based systems have recently emerged as biological drug carriers; examples include erythrocytes, bacterial ghosts, and genetically engineered stem and immune cells[26,27]. Among them, platelets are anucleated cellular fragments released from megakaryocytes and are best known for their function in hemostasis[28–31]. The average life span of circulating platelets is 8 to 9 days[27,32], which could greatly improve the pharmacokinetics of intravenously injected therapeutics. Moreover, transfused platelets could migrate to the site of surgical wounds[33], where residual tumours may survive after surgery. Emerging evidence has shown that platelets also have the capability to recognize and interact with CTCs[34–36], which are shed from the primary tumour into the bloodstream and can lead to metastases. Along with their intrinsic tendencies to accumulate at wounds and to interact with CTCs, platelets are also considered immune 'cells' that initiate and enhance many inflammatory conditions[37–39]. Platelet-derived chemokines recruit and awaken T cells as well as other immune cells. As the major source of soluble CD40L (sCD40L), platelets can boost the T-cell immune response and are necessary for inducing dendritic cell maturation and B-cell isotype switching for production of immunoglobulin G (IgG)[40]. It has also been reported that PDL1 and PDL2 are upregulated in response to inflammation[41,42], which results in PDL1-positive tumours, making the tumour more sensitive to anti-PD therapy and potentially improving the objective response rate.

In this work, inspired by the intrinsic properties of platelets, we conjugated anti-PDL1 (antibodies against PDL1; hereafter, aPDL1) to the

[1]Joint Department of Biomedical Engineering, University of North Carolina at Chapel Hill and North Carolina State University, Raleigh, North Carolina 27695, USA. [2]Division of Molecular Pharmaceutics and Center for Nanotechnology in Drug Delivery, Eshelman School of Pharmacy, University of North Carolina at Chapel Hill, Chapel Hill, North Carolina 27599, USA. [3]Department of Medicine, University of North Carolina at Chapel Hill, Chapel Hill, North Carolina 27599, USA. *e-mail: zgu@email.unc.edu

surface of platelets for use as a preventative treatment for post-surgical tumour recurrence (Fig. 1a). With the help of platelets, aPDL1 can be targeted to the cancer cells after surgery, while reducing off-target effects. We found that the binding of aPDL1 to non-activated platelets was highly stable, while release of aPDL1 could be significantly promoted on the activation of platelets. We reasoned that the aPDL1 release may result from the platelet-derived microparticles (PMPs), which are generated from the plasma membrane of activated platelets[43]. Such structural alterations can facilitate aPDL1 binding to tumour cells and APCs. By intravenous injection of aPDL1-conjugated platelets (P–aPDL1) into mice with B16 melanomas and triple-negative mammary carcinomas that had been previously resected (~1% remaining), we showed that platelets can facilitate aPDL1 transport to residual microtumours at the surgical site, and to CTCs in the blood. A T-cell-inflamed tumour microenvironment was created by the platelets on activation, leading to increased PDL1 expression at the tumour site. aPDL1 was effectively released after platelet activation, thereby blocking PDL1 on tumour and APCs. Our results show that platelets have promise as a means of targeted, controlled delivery of aPDL1 for the prevention of cancer recurrence post surgery.

Engineering platelets decorated with aPDL1

A covalent approach was employed to conveniently conjugate aPDL1 to platelets via a bifunctional maleimide linker, which bypasses the need for genetic modification[44]. The binding of aPDL1 to platelets was validated using immunofluorescence (Supplementary Fig. 1). In addition, the maleimide-free aPDL1 showed minimal nonspecific binding to the platelets (Supplementary Fig. 2). The enzyme-linked immunosorbent assay (ELISA) showed that platelets could be readily coupled with aPDL1, at up to ~0.3 pg per platelet (Supplementary Fig. 3a). We found that coupling 0.1 and 0.2 pg of aPDL1 per platelet had no obvious effect on their viability (Supplementary Fig. 3b). Such covalent binding was highly stable, and did not show significant release within two days (Supplementary Fig. 3c). Furthermore, several platelet surface proteins, which modulate cell adhesion and migration, were examined after platelet decoration and we did not find any significant changes in these proteins (Supplementary Fig. 4). Overall, conjugation of aPDL1 did not induce any significant damage in the decorated platelet cells.

Activation of platelets promotes aPDL1 release

Platelet activation happens after adhesion occurs[45]. A platelet contains about 60 granules, which in turn contain many molecules with immune functions[38]. On platelet activation, the granules release these immunoactive molecules into the extracellular environment, leading to recruitment and activation of other immune cells, and induction of T-cell migration and monocyte differentiation into dendritic cells. In addition, PMPs are generated from the plasma membrane on platelet activation[43]: activated platelets release PMPs carrying adhesion molecules and chemokines, facilitating monocyte traps at the site of PMP deposition[46]. To examine whether P–aPDL1 could be activated on stimulation, we used thrombin to activate them *in vitro*. Transmission electron microscopy (TEM) images of P–aPDL1, before and after activation, indicated that large numbers of PMPs were generated (Fig. 1b, Supplementary Fig. 5). It was also observed that the platelet morphology became more dendritic and expansive. More interestingly, significant release of aPDL1 from the activated platelets was found using ELISA (Fig. 1c). The remarkable aPDL1 release was ascribed to PMPs that were dissociated from the plasma membrane on platelet activation. To test this hypothesis, immunofluorescence imaging of activated P–aPDL1 was carried out. Platelets were stained with calcein and aPDL1 was stained with a fluorescent secondary antibody (Supplementary Fig. 6). It was found that the aPDL1 was present on the PMPs after activation of platelets.

Several pro-inflammatory cytokines were released with aPDL1 after platelet activation (Fig. 1d,e). To further validate the aPDL1 release from the platelets via PMP generation, a transwell culture system was used. P–aPDL1 were cultured in the upper compartment of the transwell culture system, while B16 cancer cells were grown in the lower compartment (Supplementary Fig. 7). The micropores in the insert membrane had a diameter of 1 μm, allowing PMPs to cross the membrane freely. The cancer cells were co-incubated with non-activated and activated platelets for 12 h before immunostaining. As shown in Fig. 1f and Supplementary Fig. 7, a large amount of aPDL1 was bound to the cancer cell membranes where the platelets had been activated; whereas, very little binding (fluorescence) was detected in the wells with non-activated platelets. Collectively, the data suggest that aPDL1 is released from activated platelets and that it binds to cancer cells.

In vivo P–aPDL1 therapy

Coupling of aPDL1 to the surface of platelets has the potential to alter their *in vivo* behaviour. Therefore, the *in vivo* pharmacokinetics of P–aPDL1, following systemic administration, was evaluated in healthy mice. A solution of free aPDL1 or a suspension of P–aPDL1, or a mixture of unconjugated platelets and free a-PDL1, were intravenously injected into the mice using equivalent aPDL1 doses. ELISA analysis of the blood showed that the circulation half-life for aPDL1 was greatly increased when it was linked to the platelets: 34.8 h versus 5.2 h and 5.5 h for the free-aPDL1 solution and the mixture, respectively (Fig. 2a). The relatively short blood-circulation time compared with other therapeutic antibodies in clinical use is attributable to the higher immunogenicity and nonspecific binding of the rat anti-mouse IgG. We then tested their capacity to accumulate at the wound site, after incomplete removal of the primary tumour by surgery. aPDL1 was fluorescently labelled using Cy5.5 and then conjugated to platelets. *In vivo* fluorescence imaging was conducted 2 h post injection of the P–aPDL1 or free aPDL1, with major organs collected for *ex vivo* fluorescence imaging (Supplementary Fig. 8). It was observed that aPDL1 was enriched around the surgical wound and residual tumours when it was conjugated to the platelets, whereas insignificant fluorescence signal was detected at the wound site for the free aPDL1 (Fig. 2b). *Ex vivo* imaging of major organs, as well as the wounds with residual microtumours, further confirmed the accumulation of P–aPDL1 at the target sites (Fig. 2c, Supplementary Fig. 8). The predominant aPDL1 fluorescence was in the liver, but the P–aPDL1 showed significantly lower fluorescence here despite the equivalent dose, suggesting a longer blood circulation time for P–aPDL1. Moreover, P–aPDL1-treated mice showed 9.4-fold greater fluorescence around the surgical wound and residual microtumours than those treated with the free aPDL1; at 2 h post intravenous (i.v.) injection (Fig. 2d). Confocal images of microtumour slices also indicated significantly increased tumour uptake of aPDL1 when conjugated to platelets (Fig. 2e, Supplementary Fig. 9a). Furthermore, aPDL1 released from platelets was clearly observed *in vivo* via fluorescence imaging (Supplementary Fig. 9b). The haemostatic effect of modified platelets was also examined, and we found that mouse tail bleeding time did not significantly differ between mice receiving P–aPDL1 and those receiving undecorated (naïve) platelets (Supplementary Fig 10).

To examine the effect of platelet injection on local and systemic inflammation *in vivo*, we assessed the levels of pro-inflammatory cytokines after surgical removal of the primary tumour, and i.v. injection of platelets. Six hours post injection, wound tissue and serum were collected, and the tissue was cultured in medium for 24 h. After examination of this medium, it was found that levels of the cytokines, IL1β, IL6, TNFα and sCD40L, were all elevated versus those of the untreated-control (no surgery) and wound-bearing (surgery alone) mice (Supplementary Fig. 11a). In contrast, the serum levels were not increased by the platelets (Supplementary Fig. 11b), so our results suggest that the injection of platelets induced a local pro-inflammatory environment at the surgical site, without causing systemic inflammation.

A pro-inflammatory tumour environment facilitates aPDL1 immunotherapy by converting quiescent precursor lymphocytes into activated lymphocytes[47]. Consistent with this, we found that expression of PDL1 was upregulated at the tumour site in both the tumour cells and tumour-infiltrating immune cells, perhaps as a result of the platelet-induced pro-inflammatory environment (Supplementary Fig. 11c,d). The increased number of PDL1-positive cells within the tumour should further enhance the anti-PDL1 immunotherapy and potentially increase the objective response rate[41,42].

To investigate P–aPDL1 treatment of residual microtumours that remain after surgery, we used the B16F10 mouse melanoma incomplete-tumour-resection model to mimic post-surgical local recurrence (Fig. 2f). After surgically removing most of the tumour (~99%), the mice were intravenously injected with a single dose of phosphate-buffered saline (PBS), platelets, aPDL1 or P–aPDL1 (aPDL1 = 1 mg kg^{-1}). Tumour growth was monitored via the bioluminescence of B16F10 cells. We found that the mice receiving P–aPDL1 exhibited the smallest relapsed-tumour volumes, with 6 of 8 in this group showing strong responses without any detectable tumour. In contrast, those treated with free aPD1 showed a modest delay of tumour growth but recurrence was not prevented in the surgical bed. When unconjugated platelets alone were used, tumour recurrence was similar to that in the PBS controls (Fig. 2g,h). The mouse survival rate, which was correlated with tumour size (Fig. 2i), was about 75% after 60 days for mice receiving P–aPDL1. In stark contrast, no mice survived beyond day 30 for all other groups (Fig. 2j).

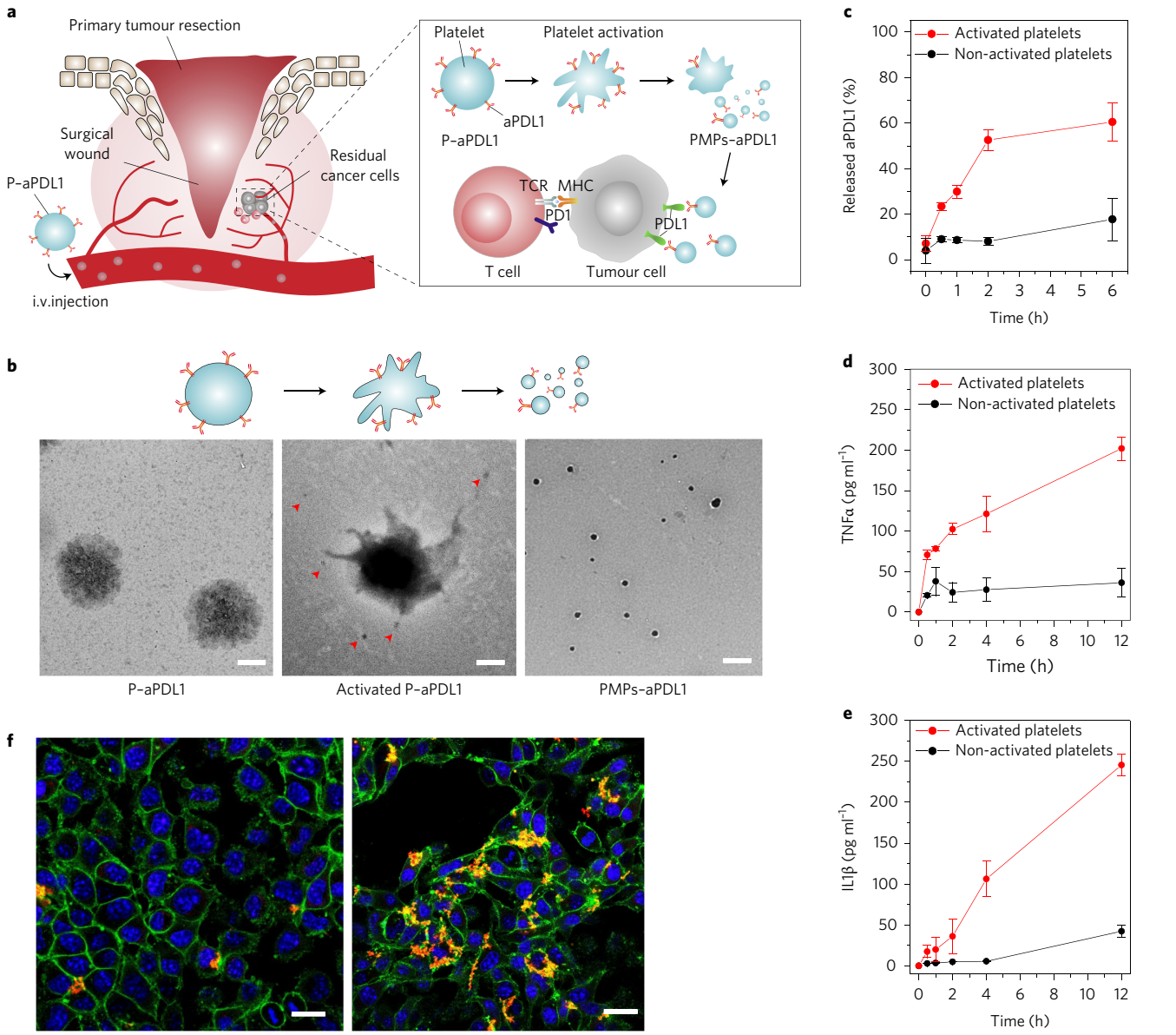

Figure 1 | *In situ* activation of P–aPDL1 promoted release of anti-PDL1 (aPDL1) and cytokines. a, Schematic illustration of the delivery of aPDL1 to the primary-tumour resection site by platelets, where TCR is T cell receptor and MHC is major histocompatibility complex. **b**, TEM images of P–aPDL1 before (left) and after (middle and right) activation. The red arrowheads indicate PMPs released from the platelet; a large number of these were observed via electron microscopy. Scale bars, 0.5 μm. **c**, Percentage of aPDL1 released from non-activated and activated platelets at different time points. **d**,**e**, Amount of TNFα and IL1β released from non-activated and activated platelets at different time points. **f**, Confocal immunofluorescence images of B16 cancer cells co-incubated with non-activated (left) and activated (right) P–aPDL1 in a transwell system (pore size, 1 μm). P–aPDL1 and B16 cancer cells were cultured in upper and lower compartments, respectively. Red, blue and green fluorescence indicate aPDL1, nucleus and plasma membrane, respectively. Scale bars, 20 μm. Error bars represent the s.d. of three independent experiments ($n = 3$).

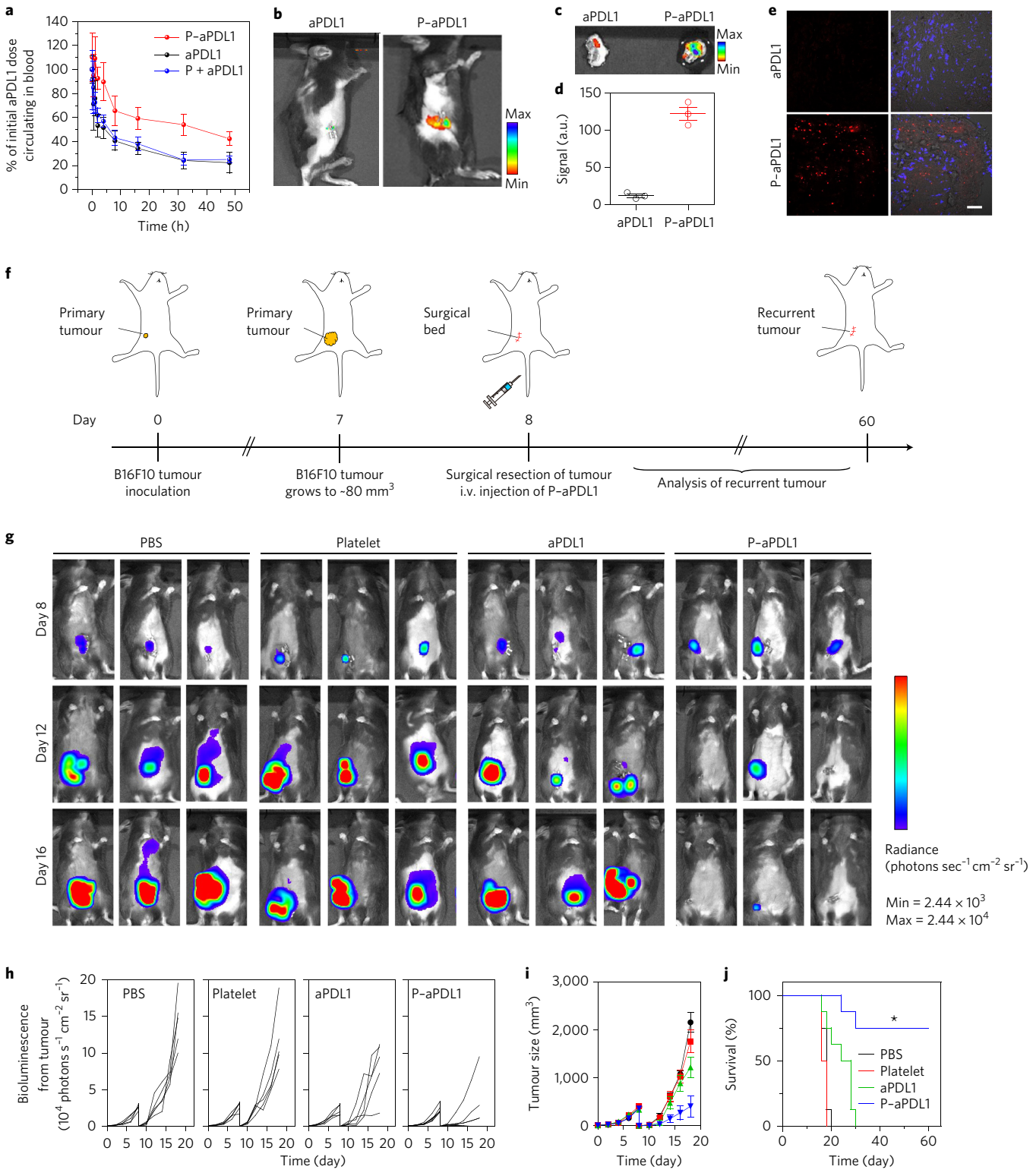

Figure 2 | P–aPDL1 reduced *in vivo* recurrence of melanoma tumours in the surgical bed. a, Time course of anti-PDL1 (aPDL1) levels in blood after mice were injected with P–aPDL1, free aPDL1 or a platelets + aPDL1 mixture. Error bars represent the s.d. of three independent experiments ($n = 3$). **b**, Fluorescence imaging (aPDL1–Cy5.5) of the mice 2 h after i.v. injection of P–aPDL1 or an equivalent dose of free aPDL1. **c**, *Ex vivo* imaging of wounds with residual tumours 2 h after i.v. injection of P–aPDL1 or free aPDL1. **d**, The mean aPDL1–Cy5.5 fluorescence intensities in the wounds shown in **c**. Error bars represent the s.e.m. of triplicate samples. **e**, Confocal images of slices from residual tumours taken from the mice shown in **b**. Blue and red fluorescence indicates the nucleus and aPDL1, respectively. Scale bar, 20 μm. **f**, Schematic illustrating the use of P–aPDL1 therapy in an incomplete-surgery tumour model. **g**, *In vivo* bioluminescence imaging of B16F10 tumours after removal of the primary tumour. Three representative mice per treatment group are shown. **h**, Quantified bioluminescence for tumours from the different treatment groups. **i**,**j**, Tumour growth (size) and survival curves; there were eight mice per treatment group for the survival study. Error bars represent the s.e.m. $^*P < 0.05$.

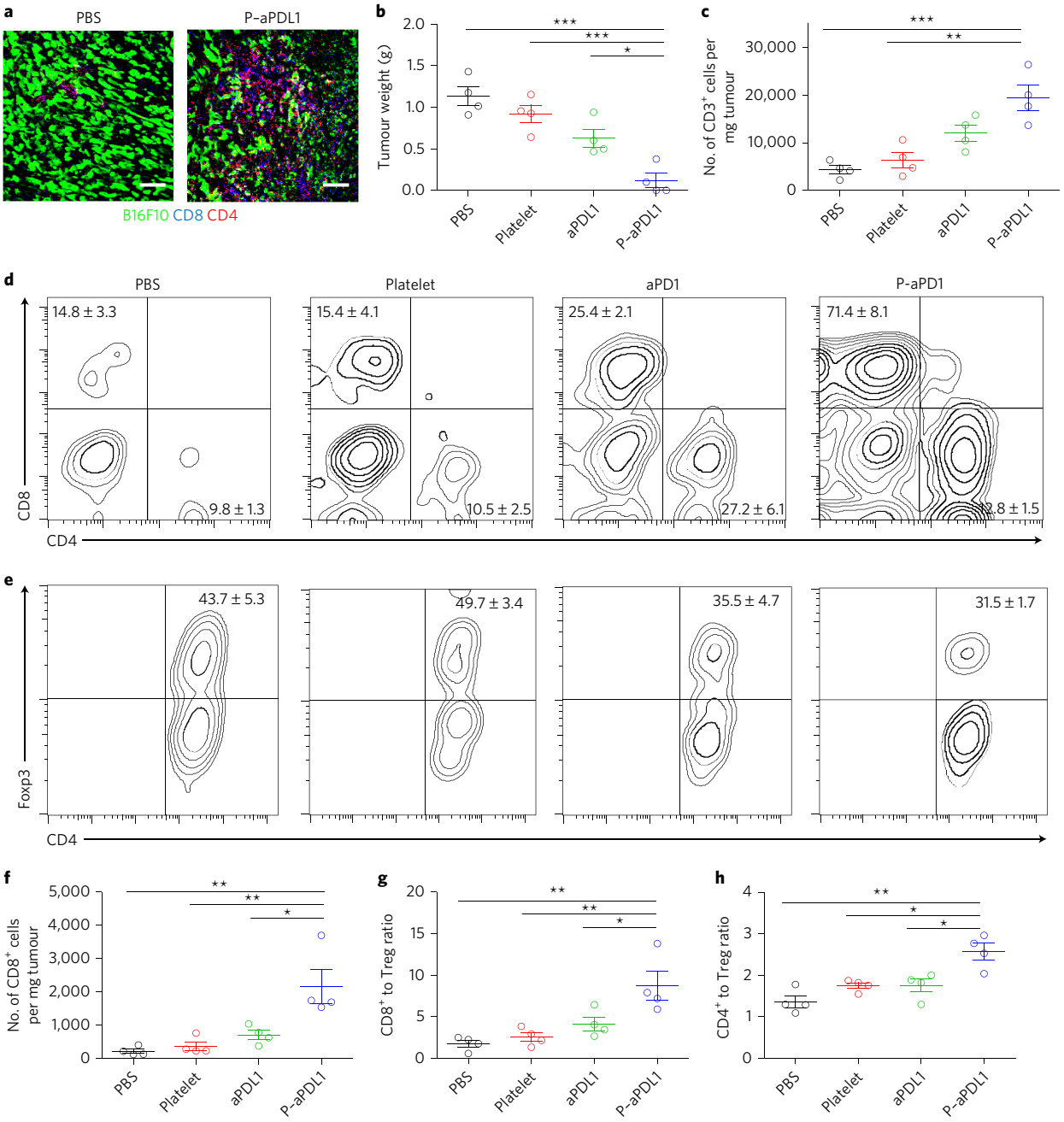

Figure 3 | P–aPDL1 triggered a robust, T-cell-mediated anti-tumour immune response. a, Immunofluorescence of residual tumours showed CD4⁺ T cells and CD8⁺ T cells infiltration. Scale bar, 50 μm. **b**, Tumour weights. **c**, Number of CD3⁺ cells per mg of tumour after treatment. The error bars represent the s.e.m. ($n=4$). **d**, Number of CD4⁺ and CD8⁺ T cells as a percentage of the total CD3⁺ cell population, and representative dot plots for residual tumours treated as indicated. The higher cell numbers in all four quadrants indicate much more CD3⁺ tumour-infiltrating lymphocytes at the tumour site. **e**, Number of CD4⁺ Foxp3⁺ T cells as a percentage of the total CD3⁺ cell population, and representative dot plots for residual tumours treated as indicated. **f**, Number of the CD8⁺ cells per mg of tumour after treatment. **g**,**h**, Ratios of tumour-infiltrating CD8⁺ T cells and CD4⁺ effector T cells versus regulatory T cells in the residual tumours after treatment. Error bars represent the s.e.m. ($n=4$). Statistical significance was calculated via one-way ANOVA with a Tukey post-hoc test. $^{*}P<0.05$; $^{**}P<0.01$; $^{***}P<0.005$.

T-cell-mediated immune responses

Tumour-infiltrating lymphocytes (TILs) from the recurrence tumours were harvested and analysed via immunofluorescence and flow cytometry on day 16. Immunofluorescence staining revealed that the residual tumours in the control group had limited T-cell infiltration. In contrast, those from P–aPDL1-treated mice were highly infiltrated by both CD8⁺ and CD4⁺ T cells (Fig. 3a, Supplementary Fig. 12). The tumour weights were significantly lower in the P–aPDL1-treated mice on day 16 (Fig. 3b), which was associated with an increase in the absolute number of CD3⁺ cells in the residual tumour (Fig. 3c). More importantly, the absolute number of CD8⁺ T cells, per gram of tumour, increased by almost tenfold in the P–aPDL1-treated mice versus the PBS controls, and threefold over the free-aPDL1-treated mice (Fig. 3d–f).

Tumour-infiltrating CD4⁺ Foxp3⁺ T cells were also examined (Fig. 3e). Intratumoural ratios of effector to regulatory T cells were significantly enhanced in mice after P–aPDL1 therapy (Fig. 3f–h). In addition, proliferation of CD8⁺ and CD4⁺ effector T cells was

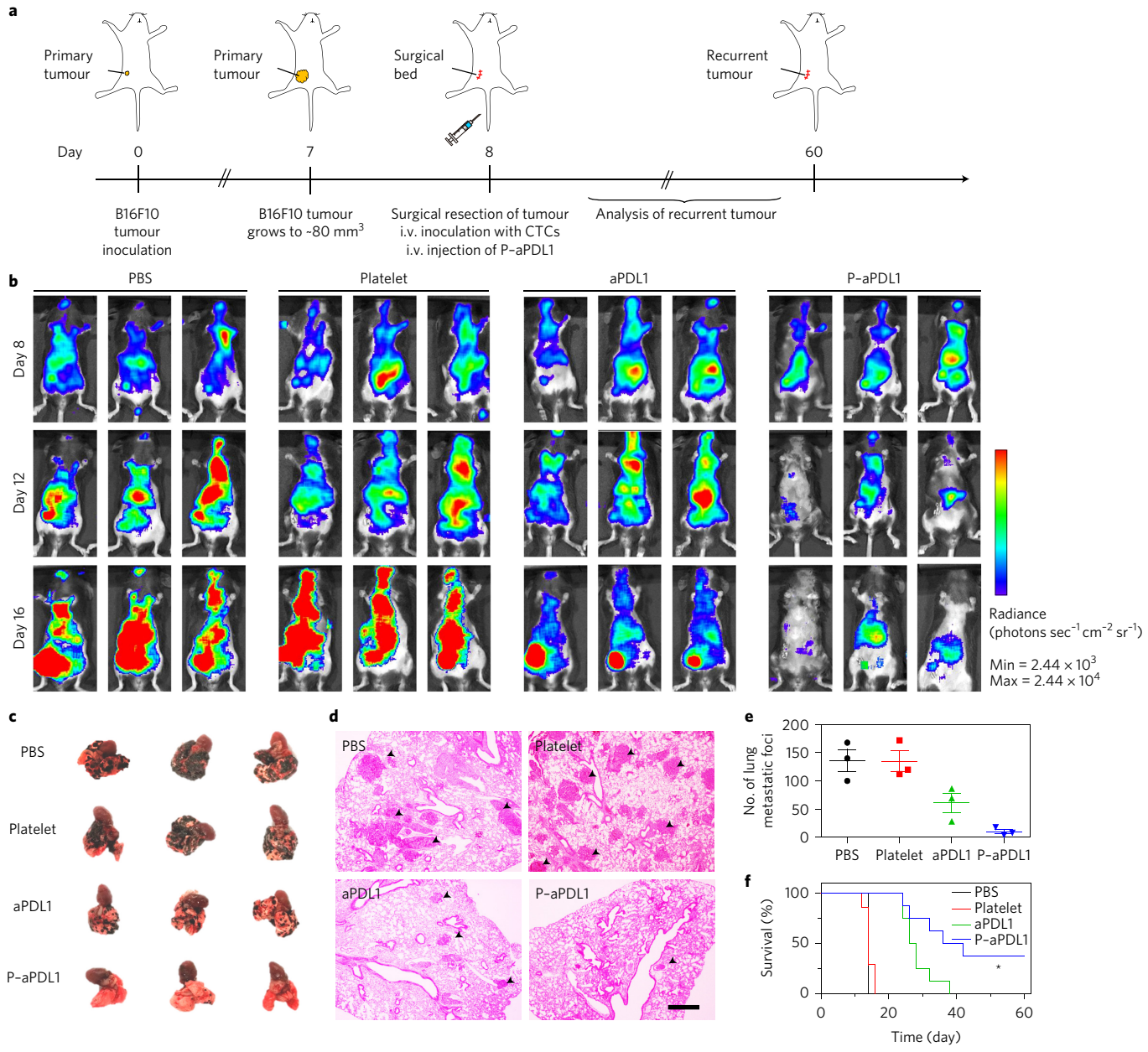

Figure 4 | P–aPDL1 reduced metastasis and local recurrence of melanoma. a, Schematic illustrating P–aPDL1 therapy in a mouse model of incomplete resection and metastasis. **b**, *In vivo* bioluminescence imaging of B16F10 metastasis for different treatment groups (three representative mice shown per group). **c**,**d**, Representative lung photographs (**c**) and H&E-stained lung slices (**d**) collected from the mice after indicated treatments. The black arrowheads mark metastatic tumours in the lung. Scale bar, 500 μm. **e**, Numbers of lung metastatic foci after different treatments (mean ± s.e.m.; $n = 3$). **f**, Survival curves for different treatments (seven or eight mice per treatment group; $n = 7$ or 8). $^*P < 0.05$.

high within the tumours of P–aPDL1-treated mice, as measured by the expression of the cell-cycle associated protein, Ki67. In contrast, P–aPDL1 therapy did not significantly increase proliferation of tumour-infiltrating regulatory T cells (Supplementary Fig. 13). Taken together, these observations suggested that P–aPDL1 could effectively deliver aPDL1 to the tumour microenvironment, triggering a robust T-cell-mediated anti-tumour immune response.

P–aPDL1 therapy for metastatic disease

To examine the potential of P–aPDL1 to treat CTCs, we first tested it in an experimental metastasis model by intravenously injecting mice with B16F10 cells after surgery, thereby mimicking the escape of CTCs from the primary tumour and into circulation[48] (Fig. 4a, Supplementary Fig. 14). The mice were injected (i.v.) with a single dose of PBS, platelets, aPDL1 (aPDL1 = 1 mg kg^{-1} or 2 mg kg^{-1}) or P–aPDL1 (aPDL1 = 1 mg kg^{-1}), immediately after surgery. Based on the bioluminescence of the B16F10 cells in the mice (Fig. 4b, Supplementary Fig. 14), it was found that the free-aPDL1 treatment reduced metastatic cancer, but did not significantly reduce local tumour recurrence at the surgical site, even at the higher dose of 2 mg kg^{-1}; this was possibly due to the poor accumulation of aPDL1 in and around these residual microtumours after surgery (Supplementary Fig. 8). In contrast, P–aPDL1 therapy substantially reduced both local tumour recurrence and lung metastasis; as was confirmed by observation of the whole lungs (Fig. 4c), hematoxylin and eosin (H&E) staining (Fig. 4d) and fluorescence imaging (Supplementary Fig. 15). The average number of metastatic sites in the lungs decreased greatly when the P–aPDL1 treatment was

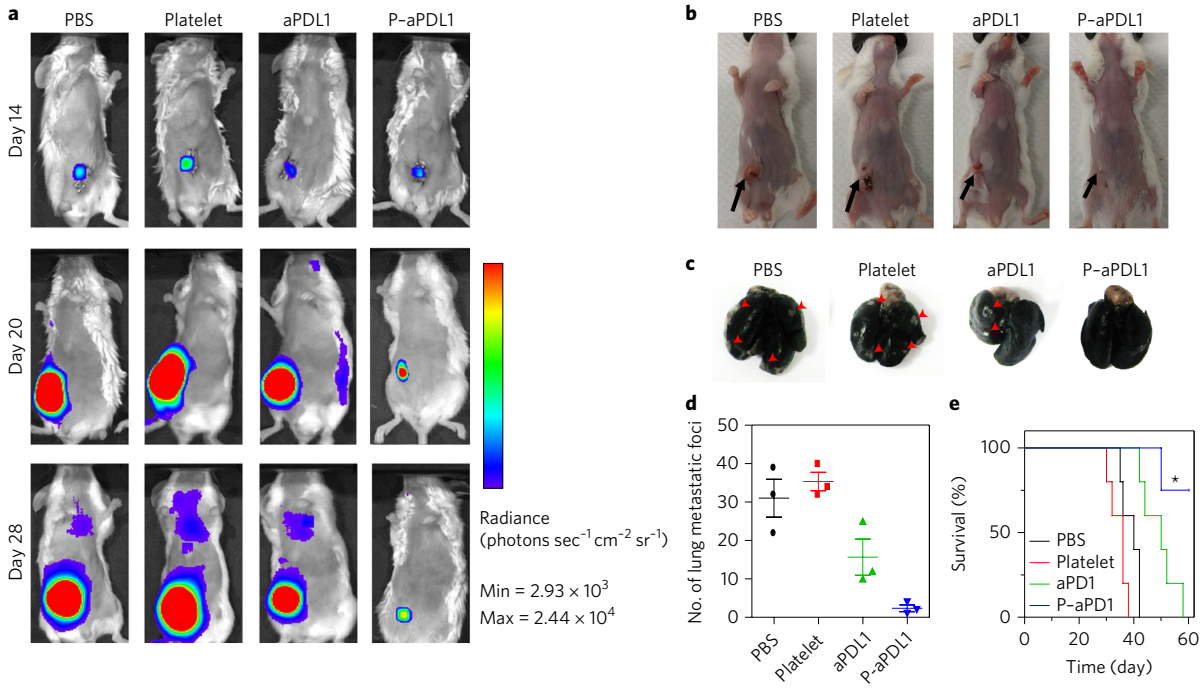

Figure 5 | P-aPDL1 treatment of recurrent triple negative 4T1 tumour. a, *In vivo* bioluminescence imaging of 4T1 metastasis for different treatments. **b**, Representative images of mice two weeks after surgery. Black arrows indicate the recurrent tumour in the surgical bed. **c**, Representative lung photographs collected from the mice after different treatments. Red arrowheads indicate tumour foci in the lung. **d**, Numbers of lung metastatic foci after different treatments (mean ± s.e.m.; $n = 3$). **e**, Survival curves for different treatments (eight or ten mice per treatment group; $n = 8$ or 10). $^*P < 0.05$.

given (Fig. 4e). Furthermore, the survival time of the treated mice was significantly increased when compared with the control group (Fig. 4f). The improved anticancer effects of P–aPDL1 versus free aPDL1 can be partly attributed to the increased local concentration of antibodies around the cancer cells (Supplementary Fig. 8). Another component of the enhanced effect was platelet activation, as it not only induced release of the conjugated aPDL1, but also helped recruit many other immune cells to infiltrate the tumour microenvironment. With the PDL1 blockade, these immune cells could induce strong anticancer immune responses.

To further verify whether *in situ* activation of P–aPDL1 contributed to the anticancer effects, PMPs were collected from the platelets and modified with aPDL1 (Supplementary Figure 14.). Direct injection of these microparticles (separate from the platelets) clearly limited the anticancer effect, so that it was no greater than that for free-aPDL1 (Fig. 4). This could be explained by previous studies reporting that PMPs can be cleared rapidly following introduction into the circulation[49,50]. These results suggest that *in situ* activation of P–aPDL1 at the tumour site was an essential component of its anticancer effect.

P–aPDL1 therapy for recurrence of triple-negative carcinoma

To assess the effectiveness of P–aPDL1 in reducing another type of cancer recurrence after surgery, we performed tests in a triple-negative breast cancer (TNBC) tumour model (4T1 carcinoma). BABL/c mice were subcutaneously injected with triple-negative 4T1 tumour cells, and 14 days later, the primary tumour was surgically removed, leaving residual microtumours behind (~1% of original tumour mass). Therapeutic platelets decorated with aPDL1 were intravenously injected into the mice immediately after surgery. In this model, a single course of P–aPDL1 therapy was sufficient to reduce the growth of the residual tumour (Fig. 5a,b). Furthermore, the therapy was also very effective on lung metastases: only a few metastatic foci (median, ~2) were found in the lungs of the P–aPDL1 treated mice, whereas a median of 16 foci were found in the free-aPDL1 group, and the medians for the platelet-treated and PBS groups were ~30 (Fig. 5c,d). Mice receiving P–aPDL1 therapy after surgery also benefitted greatly in terms of their survival rate, with 75% of them still alive 60 days post tumour inoculation (Fig. 5e). In contrast, the PBS and platelet groups hit 0% around day 40, while the aPDL1 mice lasted longer but were all dead by day 60.

In summary, our strategy used *in situ* activation of platelets to enhance the delivery and effectiveness of aPDL1 in mice, thereby greatly reducing the presence of residual tumour cells after surgery, and hence also disease recurrence. Such a P–aPDL1 therapy could substantially improve the effectiveness of surgical interventions by reducing the risk of cancer recurrence and metastasis after resection of the primary tumour. Beyond the specific use of platelets for aPDL1 delivery, this method may inspire new treatments that apply bioparticulates for targeted delivery and bioresponsive release of therapeutics[51].

Methods

The experiments did not use a method of randomization. The investigators were not blinded to allocation during experiments and outcome assessment.

Cell lines. The mouse melanoma cell line, B16F10, and mouse mammary carcinoma cell line, 4T1, were purchased from the American Type Culture Collection. B16F10-luc-GFP and 4T1-luc-GFP cells were gifts from L. Huang at the University of North Carolina at Chapel Hill. The B16F10 cells were maintained in Dulbecco's modified Eagle medium (Gibco, Invitrogen) supplemented with 10% fetal bovine serum (Invitrogen), 100 U ml^{-1} penicillin (Invitrogen), and 100 U ml^{-1} streptomycin (Invitrogen). The 4T1 cells were maintained in RPMI-1640 medium (Gibco, Invitrogen) supplemented with 10% fetal bovine serum (Invitrogen), 100 U ml^{-1} penicillin (Invitrogen) and 100 U ml^{-1} streptomycin (Invitrogen). Master and working cell banks were generated immediately on receipt. The third and fourth passages were used for tumour experiments. Cells were tested every three months for potential mycoplasma. Re-authentication of cells was not performed after receipt.

Mice. C57BL/6 mice and BALB/c mice were purchased from Jackson Lab. Age-matched (6–10 weeks) female animals were used throughout all experiments. We performed all mouse studies in the context of the animal protocol approved

by the Institutional Animal Care and Use Committee at the University of North Carolina at Chapel Hill and North Carolina State University. Experimental group sizes were approved by the regulatory authorities for animal welfare after being defined to balance statistical power, feasibility and ethical aspects. All mice were kept in accordance with federal and state policies on animal research at the University of North Carolina at Chapel Hill and North Carolina State University.

Antibodies. The anti-PDL1 antibody (aPDL1) used *in vivo* was purchased from Biolegend (cat. no. 124329, Clone: 10F.9G2). The primary antibodies used for immunostaining were against CD3 (Thermo Fisher Scientific, cat. no. A18644), CD4 (Thermo Fisher Scientific, cat. no. A18667), CD8 (Thermo Fisher Scientific, cat. no. A18609), PD1 (Biolegend, cat. no. 135227), CD11c (Biolegend, cat. no. 117309), PDL1 (Biolegend, cat. no. 124311), CD20 (Biolegend, cat. no. 150411), CD11b (Biolegend, cat. no. 101211), CD9 (Biolegend, cat. no. 124805), CD41 (Biolegend, cat. no. 133905), CD61 (Biolegend, cat. no. 104307), CD62P (Biolegend, cat. no. 148305), CD40L (Biolegend, cat. no. 106505), intracellular Ki67 (Biolegend, cat. no. 652405), and intracellular Foxp3 (eBioscience, cat. no. 71-5775-40) for fluorescence-activated cell sorting (FACS analysis following the manufacturers' instructions. The stained cells were analysed on a CytoFLEX flow cytometer (Beckman), using the FlowJo software package (version 10.0.7; TreeStar, USA, 2014). The secondary antibodies used for immunostaining were goat anti-rat IgG (H + L; Thermo Fisher Scientific, cat. no. A18866), rabbit anti-rat IgG (H + L; Thermo Fisher Scientific, cat. no. A18920) and goat anti-rat IgG (minimal cross-reactivity; Biolegend, cat. no. 405408).

Preparation of aPDL1 conjugated platelets. Murine platelets were isolated as described previously[52]. In brief, whole blood was collected from the C57BL/6 or BALB/c mice (non-terminal collection from the orbital sinus or saphenous vein; 20 mice were used) into a plastic syringe containing 1.0 ml citrate-phosphate-dextrose (16 mM citric acid, 90 mM sodium citrate, 16 mM NaH_2PO_4, 142 mM dextrose, pH 7.4) and centrifuged at 100 *g* for 20 min at room temperature. The platelet-rich plasma (PRP) was transferred to a separate tube using a transfer pipette (wide orifice), and PGE1 was added to each tube at a final concentration of 1 μM. (Note that if the PRP has a reddish colour, discard these samples.) Platelets were isolated from the PRP via centrifugation at 800 *g* for 10 min. The plasma was discarded, and the platelets were resuspended carefully and slowly in Tyrode's buffer (134 mM NaCl, 12 mM $NaHCO_3$, 2.9 mM KCl, 0.34 mM Na_2HPO_4, 1 mM $MgCl_2$, 10 mM HEPES, pH 7.4) or PBS with PGE1 added at 1 μM. Note that this buffer was released slowly along the tube wall, while minimizing agitation. Each *in vivo* injection required 500–600 μl whole blood.

The surface of the platelets was functionalized with aPDL1 in three steps. First, 100 μl of platelets (1×10^8) was resuspended in 400 μl of PBS (pH 8), including PGE1 (1 μM), and incubated with 0.1 mg ml^{-1} Traut's Reagent (2-iminothiolane; Pierce) for 30 min at room temperature. After 30 min of reaction, the excess Traut's Reagent was removed by centrifugation at 800 *g* for 10 min and washed with Tyrode's buffer (with PGE1 added at 1 μM) three times (without resuspension to avoid unnecessary platelet activation). In the meantime, aPDL1 was mixed with sulfosuccinimidyl-4-(*N*-maleimidomethyl)- cyclohexane-1-carboxylate (Sulfo-SMCC, Pierce) in PBS (pH 7.4) at a molar ratio of 1:1.2 for 2 h at 4 °C. The excess Sulfo-SMCC was removed using a centrifugal filter device (molecular weight cut-off = 10 kDa) to purify the SMCC activated antibody. Lastly, platelets and antibodies were mixed in Tyrode's buffer (+ PGE1 at 1 μM). After 2 h at room temperature, the excess antibodies were removed by centrifugation at 800 *g* for 10 min. The precipitate fraction was retained and washed with Tyrode's buffer (+ PGE1 at 1 μM) twice. Platelet recovery was higher than 80% after conjugation based on the platelet count analysis. The obtained aPDL1–platelets were stored in Tyrode's buffer (+ PGE1 at 1 μM) at room temperature prior to use in experiments. Unconjugated platelets were not separated from conjugated platelets. The amount of aPDL1 conjugated to the platelets was measured via ELISA (rat IgG total ELISA kit, eBioscience, cat. no. 88-50490-22). Freshly isolated platelets were used within 6 h. The platelet-activation marker, CD62P, was used for evaluating platelet activation. All platelet manipulations were performed at room temperature.

To study the conjugation efficiency, various amounts of aPDL1 were added to the platelets for conjugation. Unconjugated aPDL1 was removed with the supernatant after centrifugation at 800 *g* for 10 min. The P–aPDL1 pellet was then washed twice with Tyrode's buffer (+ PGE1 at 1 μM), using centrifugation at 800 *g* for 10 min. After that, the P–aPDL1 was resuspended in 100 μl deionized water and ultrasonicated to lyse the platelets and release the aPDL1. The amount of aPDL1 conjugated to the platelets was measured using ELISA. The efficiency of aPDL1 conjugation to platelets (conjugated aPDL1 as a percentage of total aPDL1 added) was about 75% when 0.2 pg aPDL1 per platelet was added. To assess the stability of the platelets after decoration with aPDL1, platelet counts were determined at 0 h and 24 h. To study the stability of aPDL1 on platelets over time, the platelets were stored in Tyrode's buffer (+ PGE1 at 1 μM) at room temperature. At different times, 50 μl P–aPDL1 was extracted. Released aPDL1 in the supernatant was removed by centrifugation at 800 *g* for 10 min. The conjugated platelets were suspended in 100 μl deionized water and ultrasonicated to release the aPDL1. The amount of aPDL1 conjugated to the platelets was measured via ELISA. To activate the platelets, 0.5 U thrombin ml^{-1} were added to the platelet suspension. PGE1 was removed prior to platelet activation. Platelets were activated for 30 min at 37 °C.

PMPs were prepared from platelets as previously described[53]. Before the experiments, platelet concentrates were activated by thrombin (2 U ml^{-1}) for 30 min and centrifuged at 800 *g* for 10 min. The PMP-enriched supernatants were then collected and examined via antibodies for mouse aIIbb3 and CD62P (P-selectin) combined with flow cytometry. Next, aPDL1 was conjugated to the PMPs as described above. The conjugation efficiency and stability were examined using ELISA.

Transmission electron microscopy. To prevent morphological changes occurring in the subsequent preparation steps, the platelets were fixed by suspending them in 10% buffered formaldehyde solution. Immediately afterwards, the samples were centrifuged at 800 *g* for 10 min at room temperature. After discarding the supernatant, platelets were fixed with 2.5% glutaraldehyde in the cacodylate buffer (pH 7.2) for 90 min at 4 °C (for activated platelets, the supernatant were also collected for TEM imaging). After fixation, the platelets were washed twice using centrifugation at 800 *g* for 10 min at 4 °C. They were then sequentially stained with 2% uranyl acetate and lead citrate for 5 min each and then transferred to a copper grid[54]. The TEM images were obtained using a JEOL 2000FX instrument at 80 kV.

aPDL1 and cytokine release from platelets. To activate P–aPDL1, 0.5 U thrombin ml^{-1} was added to the suspension (~1×10^8 platelets in 500 μl Tyrode's buffer; $n = 3$) for 30 min at 37 °C. At different times, 50 μl samples of P–aPDL1 were extracted. Supernatants containing aPDL1 and cytokines released from the platelets were collected by centrifugation at 800 *g* for 10 min. Non-activated P–aPDL1 was used as a control. The amount of aPDL1 and cytokines in the supernatants was measured using ELISA (eBioscience, cat. Nos. 88-50490-22 (rat IgG), 88-7013-22 (IL1β), 88-7064-22 (IL6), 88-7324-22 (TNF-α), BMS6010 (sCD40L)). The absorbance was read on an Infinite 200 PRO plate reader.

***In vivo* pharmacokinetics.** Three mice were intravenously injected with free aPDL1, P–aPDL1 or unconjugated platelets + a-PDL1 mixture (aPDL1, 2 mg kg^{-1}, platelets, 2×10^8, in 200 μl PBS for each mouse). A 10 μl sample of blood was extracted from the tail at different time points using an anticoagulation tube. Each sample was dissolved in 100 μl water (Sigma, cat. no. W4502) and treated with ultrasound for cell lysis to release the conjugated aPDL1. The aPDL1 was measured by rat IgG total ELISA kit (eBioscience, cat. no. 88-50490-22). For the *in vivo* biodistribution study, after removal of primary tumour with ~1% residual tissue left behind, the mice were intravenously injected with Cy5.5-labelled free aPDL1 or P–aPDL1. *In vivo* fluorescence images were recorded using an IVIS Spectrum system (Perkin Elmer; manufacturer-excitation/emission filters for Cy5.5; exposure time = 1 s). For *ex vivo* imaging, treated mice were sacrificed at 2 h post injection. Major organs and tissues were collected and imaged using the same IVIS system and settings.

***In vivo* tumour models.** To measure the effects on cancer recurrence, 7 days after 1×10^6 B16F10 (or 4T1) or luciferase-tagged B16F10 (or 4T1) tumour cells were transplanted into the right flank of mice; the resulting tumours were ~300 mm^3 in volume. These tumours were then resected, leaving about 1% residual tumour tissue behind to mimic the presence of residual microtumours in the surgical bed[3]. Briefly, animals were anesthetized in an induction chamber using isoflurane (up to 5% for induction; 1–3% for maintenance), and anaesthesia was maintained via a nose cone. The tumour area was clipped and aseptically prepped. Sterile instruments were used to remove approximately 99% of the tumour. The wound was closed using an Autoclip wound closing system. For the experimental metastasis model, 1×10^5 luciferase-tagged B16F10 (or 4T1) tumour cells in 200 μL PBS were intravenously infused into mice via the tail vein after resection of the primary tumour. The mice were weighed and randomly divided into four groups of eight mice ($n = 8$). Immediately after surgery, the mice were intravenously injected with one of the treatment formulations: PBS, platelets ($1–2 \times 10^8$), aPDL1 (1 mg kg^{-1}) and P–aPDL1 (1 mg kg^{-1} aPDL1 on $1–2 \times 10^8$ platelets); the platelets were freshly prepared from healthy mice of the same strain. The tumour burden was monitored via the bioluminescence of the cancer cells. The mice were clipped and shaved using a depilatory cream before imaging. Images were taken using an IVIS Lumina imaging system (Perkin Elmer). Tumour size was measured with a digital calliper. The tumour volume (mm^3) was calculated as (long diameter × short diameter^2)/2. Metastatic burden was assessed on the basis of the bioluminescence. The lungs were weighed and micrometastases were counted. Animals were euthanized when exhibiting signs of impaired health or when the volume of the tumour exceeded 2 cm^3.

For the metastatic lung tumour in Fig. 5c, India ink was used to better visualize lung metastases following a standard protocol[55]. The mice were sacrificed and tumour burden was quantified (unblinded) after intratracheal injection of the ink (85 ml H_2O, 15 ml ink, two drops of ammonia water) and fixation with Fekete's solution (5 ml 70% ethanol, 0.5 ml formalin, 0.25 ml glacial acetic acid). After 2–6 h, tumour lesions were bleached whereas normal lung tissue remained stained.

In addition, the tumours were dissected from the mice after treatment and snap frozen in optimal cutting temperature (OCT) medium for immunofluorescence staining. Fluorescently labelled secondary antibodies were used to detect aPDL1, platelets and PMPs. For H&E staining, animals with lung tumours were sacrificed for analysis. The lung tissue sections were stained with H&E following the standard protocol[56]. All H&E staining sections were examined under an optical microscope (Leica DM5500 B).

Cytokine detection. The local and plasma levels of IL1β, IL6, TNFα and sCD40L were measured using ELISA (eBioscience). For determination of the local (wound) concentration of these cytokines 6 h after platelet injection, the wound tissue was collected and cultured at 37 °C for 24 h. Then 100 µl of medium was removed and frozen at −80 °C for analysis. For the plasma levels, about 6 h after platelet injection, plasma samples were extracted from the mice after treatment and diluted for analysis. All measurements were carried out in triplicate.

Confocal microscopy. The tumours were dissected from the mice and snap frozen in OCT medium. Several 1-µm-thick sections were cut using a cryotome and then mounted on slides. Sections were fixed in ice-cold acetone for 10 min prior to rehydration with PBS. After blocking with BSA (3%), sections were stained with primary antibodies overnight at 4 °C. Following the addition of fluorescently labelled secondary antibodies, the slides were analysed using a confocal microscope (Zeiss LSM 710).

***In vivo* bioluminescence and imaging.** Bioluminescence images were acquired using an IVIS Spectrum imaging system. Living Image software (version 4.4; Perkin Elmer, USA) was used to acquire the data 10 min after intraperitoneal injection of d-luciferin (Thermo Fisher Scientific, Pierce, Cat no. PI88291) in Dulbecco's PBS (15 mg ml^{-1}) into the animals (10 µl g^{-1} of body weight). Exposure time for the bioluminescence imaging was 5 min; to optimize reading time, bioluminescence intensity was acquired for 30 min with an exposure time of 1 min using the IVIS system. Regions of interest were quantified as the average radiance (photons s^{-1} cm^{-2} sr^{-1}) using the Living Image software.

Tail bleeding assay. Tail bleeding time was determined by removing 3 mm from the tip of the tail and then immediately immersing the tail in PBS at 37 °C. The end point was defined as the time taken for complete cessation of bleeding to occur.

Statistical analysis. All results are expressed as the mean ± s.d. or the mean ± s.e.m. as indicated. Biological replicates were used in all experiments unless otherwise stated. One-way analysis of variance (ANOVA) and Tukey post-hoc tests were used when more than two groups were compared (multiple comparisons). Survival benefit was determined using a log-rank test. All statistical analyses were performed using the Prism software package (PRISM 5.0; GraphPad Software, USA, 2007). The threshold for statistical significance was $P < 0.05$. No statistical methods were used to pre-determine the sample size of the experiments.

Data availability. Source data for the figures in this study are available on figshare at http://dx.doi.org/10.6084/m9.figshare.4231766 (ref. [57]). The authors declare that all other data supporting the findings of this study are available within the paper and the Supplementary Information.

Received 16 June 2016; accepted 17 November 2016; published 23 January 2017

References

1. Baker, D., Masterson, T., Pace, R., Constable, W. & Wanebo, H. The influence of the surgical wound on local tumor recurrence. *Surgery* **106,** 525–532 (1989).
2. Lukianova-Hleb, E. Y. *et al.* Intraoperative diagnostics and elimination of residual microtumours with plasmonic nanobubbles. *Nat. Nanotech.* **11,** 525–532 (2016).
3. Stephan, S. B. *et al.* Biopolymer implants enhance the efficacy of adoptive T-cell therapy. *Nat. Biotechnol.* **33,** 97–101 (2015).
4. Demicheli, R., Retsky, M., Hrushesky, W., Baum, M. & Gukas, I. The effects of surgery on tumor growth: a century of investigations. *Ann. Oncol.* mdn386 (2008).
5. Ceelen, W., Pattyn, P. & Mareel, M. Surgery, wound healing, and metastasis: recent insights and clinical implications. *Crit. Rev. Oncol. Hematol.* **89,** 16–26 (2014).
6. Klevorn, L. E. & Teague, R. M. Adapting cancer immunotherapy models for the real world. *Trends Immunol.* **37,** 354–363 (2016).
7. O'Sullivan, D. & Pearce, E. L. Targeting T cell metabolism for therapy. *Trends Immunol.* **36,** 71–80 (2015).
8. Robert, C. *et al.* Pembrolizumab versus ipilimumab in advanced melanoma. *N. Engl. J. Med.* **372,** 2521–2532 (2015).
9. Postow, M. A. *et al.* Nivolumab and ipilimumab versus ipilimumab in untreated melanoma. *N. Engl. J. Med.* **372,** 2006–2017 (2015).
10. Sharma, P. & Allison, J. P. The future of immune checkpoint therapy. *Science* **348,** 56–61 (2015).
11. Wang, C., Ye, Y., Hochu, G. M., Sadeghifar, H. & Gu, Z. Enhanced cancer immunotherapy by microneedle patch-assisted delivery of anti-PD1 antibody. *Nano Lett.* **16,** 2334–2340 (2016).
12. Zou, W., Wolchok, J. D. & Chen, L. PD-L1 (B7-H1) and PD-1 pathway blockade for cancer therapy: mechanisms, response biomarkers, and combinations. *Sci. Transl. Med.* **8,** 328rv4 (2016).
13. Buchbinder, E. I. & Hodi, F. S. Melanoma in 2015: immune-checkpoint blockade—durable cancer control. *Nat. Rev. Clin. Oncol.* **13,** 77–78 (2016).
14. Smyth, E. C. & Cunningham, D. Encouraging results for PD-1 inhibition in gastric cancer. *Lancet Oncol.* **17,** 682–683 (2016).
15. Rosenberg, J. E. *et al.* Atezolizumab in patients with locally advanced and metastatic urothelial carcinoma who have progressed following treatment with platinum-based chemotherapy: a single-arm, multicentre, phase 2 trial. *The Lancet* **387,** 1909–1920 (2016).
16. Naidoo, J. *et al.* Toxicities of the anti-PD-1 and anti-PD-L1 immune checkpoint antibodies. *Ann. Oncol.* **26,** 2375–2391 (2015).
17. Mellati, M. *et al.* Anti-PD-1 and anti-PDL-1 monoclonal antibodies causing type 1 diabetes. *Diabetes Care* **38,** e137–e138 (2015).
18. Boutros, C. *et al.* Safety profiles of anti-CTLA-4 and anti-PD-1 antibodies alone and in combination. *Nat. Rev. Clin. Oncol.* **13,** 473–486 (2016).
19. Larkin, J. *et al.* Combined nivolumab and ipilimumab or monotherapy in untreated melanoma. *N. Engl. J. Med.* **373,** 23–34 (2015).
20. Chen, L. & Han, X. Anti-PD-1/PD-L1 therapy of human cancer: past, present, and future. *J. Clin. Invest.* **125,** 3384–3391 (2015).
21. Weber, J. S., Kahler, K. C. & Hauschild, A. Management of immune-related adverse events and kinetics of response with ipilimumab. *J. Clin. Oncol.* **30,** 2691–2697 (2012).
22. Woo, S. R., Corrales, L. & Gajewski, T. F. The STING pathway and the T cell-inflamed tumor microenvironment. *Trends Immunol.* **36,** 250–256 (2015).
23. Hegde, P. S., Karanikas, V. & Evers, S. The where, the when, and the how of immune monitoring for cancer immunotherapies in the era of checkpoint inhibition. *Clin. Cancer Res.* **22,** 1865–1874 (2016).
24. Spranger, S. *et al.* Up-regulation of PD-L1, IDO, and Tregs in the melanoma tumor microenvironment is driven by $CD8^+$ T cells. *Sci. Transl. Med.* **5,** 200ra116 (2013).
25. Gajewski, T. F., Schreiber, H. & Fu, Y. X. Innate and adaptive immune cells in the tumor microenvironment. *Nat. Immunol.* **14,** 1014–1022 (2013).
26. Fesnak, A. D., June, C. H. & Levine, B. L. Engineered T cells: the promise and challenges of cancer immunotherapy. *Nat. Rev. Cancer* **16,** 566–581 (2016).
27. Yoo, J. W., Irvine, D. J., Discher, D. E. & Mitragotri, S. Bio-inspired, bioengineered and biomimetic drug delivery carriers. *Nat. Rev. Drug Discov.* **10,** 521–535 (2011).
28. Tamagawa-Mineoka, R. Important roles of platelets as immune cells in the skin. *J. Dermatol. Sci.* **77,** 93–101 (2015).
29. Franco, A. T., Corken, A. & Ware, J. Platelets at the interface of thrombosis, inflammation, and cancer. *Blood* **126,** 582–588 (2015).
30. Hu, C. M. *et al.* Nanoparticle biointerfacing by platelet membrane cloaking. *Nature* **526,** 118–121 (2015).
31. Textor, J. in *Platelet-Rich Plasma* (eds Lana, J. F., Santana, M. H. A., Belangero, W. D. & Luzo, A. C. M.) 61–94 (Springer, 2014).
32. Harker, L. A. *et al.* Effects of megakaryocyte growth and development factor on platelet production, platelet life span, and platelet function in healthy human volunteers. *Blood* **95,** 2514–2522 (2000).
33. Nurden, A. T., Nurden, P., Sanchez, M., Andia, I. & Anitua, E. Platelets and wound healing. *Front. Biosci.* **13,** 3532–3548 (2008).
34. Gay, L. J. & Felding-Habermann, B. Contribution of platelets to tumour metastasis. *Nat. Rev. Cancer* **11,** 123–134 (2011).
35. Nash, G. F., Turner, L. F., Scully, M. F. & Kakkar, A. K. Platelets and cancer. *Lancet Oncol.* **3,** 425–430 (2002).
36. Hu, Q. *et al.* Anticancer platelet-mimicking nanovehicles. *Adv. Mater.* **27,** 7043–7050 (2015).
37. Garraud, O. Editorial: platelets as immune cells in physiology and immunopathology. *Front. Immunol.* **6,** 1–3 (2015).
38. Morrell, C. N., Aggrey, A. A., Chapman, L. M. & Modjeski, K. L. Emerging roles for platelets as immune and inflammatory cells. *Blood* **123,** 2759–2767 (2014).
39. Semple, J. W., Italiano, J. E. & Freedman, J. Platelets and the immune continuum. *Nat. Rev. Immunol.* **11,** 264–274 (2011).
40. Elzey, B. D. *et al.* Platelet-mediated modulation of adaptive immunity: a communication link between innate and adaptive immune compartments. *Immunity* **19,** 9–19 (2003).

41. Seifert, L. *et al.* The necrosome promotes pancreatic oncogenesis via CXCL1 and Mincle-induced immune suppression. *Nature* **532,** 245–249 (2016).
42. Topalian, S. L., Drake, C. G. & Pardoll, D. M. Targeting the PD-1/B7-H1(PD-L1) pathway to activate anti-tumor immunity. *Curr. Opin. Immunol.* **24,** 207–212 (2012).
43. Siljander, P. R. M. Platelet-derived microparticles—an updated perspective. *Thromb. Res.* **127,** S30–S33 (2011).
44. Li, J., Sharkey, C. C., Wun, B., Liesveld, J. L. & King, M. R. Genetic engineering of platelets to neutralize circulating tumor cells. *J. Control. Release* **228,** 38–47 (2016).
45. Ruggeri, Z. M. & Mendolicchio, G. L. Adhesion mechanisms in platelet function. *Circ. Res.* **100,** 1673–1685 (2007).
46. Mause, S. F., von Hundelshausen, P., Zernecke, A., Koenen, R. R. & Weber, C. Platelet microparticles—a transcellular delivery system for RANTES promoting monocyte recruitment on endothelium. *Arterioscler. Thromb. Vasc. Biol.* **25,** 1512–1518 (2005).
47. Tripathi, S. & Guleria, I. Role of PD1/PDL1 pathway, and TH17 and treg cells in maternal tolerance to the fetus. *Biomed. J.* **38,** 25–31 (2015).
48. Headley, M. B. *et al.* Visualization of immediate immune responses to pioneer metastatic cells in the lung. *Nature* **531,** 513–517 (2016).
49. Flaumenhaft, R. Formation and fate of platelet microparticles. *Blood Cells Mol. Dis.* **36,** 182–187 (2006).
50. Rand, M. L., Wang, H., Bang, K. W., Packham, M. A. & Freedman, J. Rapid clearance of procoagulant platelet-derived microparticles from the circulation of rabbits. *J. Thromb. Haemost.* **4,** 1621–1623 (2006).
51. Lu, Y., Aimetti, A. A., Langer, R. & Gu, Z. Bioresponsive materials. *Nat. Rev. Mater.* **1,** 16075 (2016).
52. Cazenave, J.-P. *et al.* in *Platelets and Megakaryocytes: Volume 1: Functional Assays* (eds Gibbins, J. M. & Mahaut-Smith, M. P.) 13–28 (Methods In Molecular Biology Series Vol. 272, Humana, 2004).
53. Janowska-Wieczorek, A. *et al.* Platelet-derived microparticles bind to hematopoietic stem/progenitor cells and enhance their engraftment after transplantation. *Blood* **98,** 3143–3149 (2001).
54. Cheville, N. F. & Stasko, J. Techniques in electron microscopy of animal tissue. *Vet. Pathol.* **51,** 28–41 (2014).
55. Zimmerman, M., Hu, X. & Liu, K. Experimental metastasis and CTL adoptive transfer immunotherapy mouse model. *J. Vis. Exp.* **45,** 2077 (2010).
56. Fischer, A. H. *et al.* Hematoxylin and eosin staining of tissue and cell sections. *Cold Spring Harb. Protoc.* **5,** pdb-prot4986 (2008).
57. Wang, C. *et al. In situ* activation of platelets with checkpoint inhibitors for post-surgical cancer immunotherapy. *figshare* http://dx.doi.org/10.6084/m9.figshare.4231766 (2016).

Acknowledgements

This work was supported by grants from the Alfred P. Sloan Foundation (Sloan Research Fellowship), NC TraCS, the National Institutes of Health (Clinical and Translational Science Award (CTSA, NIH grant 1L1TR001111) to Z.G.) and a pilot grant from the University of North Carolina (UNC) Cancer Center. We acknowledge L. Huang at UNC at Chapel Hill for providing the B16F10-Luc-GFP and 4T1-Luc-GFP cell lines.

Author contributions

C.W. and Z.G. designed the project. C.W., W.S., Y.Y and Q.H. performed the experiments. All authors analysed and interpreted the data. All authors contributed to the writing of the manuscript. All authors discussed the results and implications and edited the manuscript at all stages.

Additional information

Supplementary information is available for this paper.

Reprints and permissions information is available at www.nature.com/reprints.

Correspondence and requests for materials should be addressed to Z.G.

How to cite this article: Wang, C. *et al. In situ* activation of platelets with checkpoint inhibitors for post-surgical cancer immunotherapy. *Nat. Biomed. Eng.* **1,** 0011 (2017).

Competing interests

Z.G. and C.W. have a pending patent entitled 'Platelets for delivery of cancer immunotherapeutics' (patent number, 10620-039PV1).